# Engineering the Electronic, Magnetic, and Optical Properties of GaP Monolayer by Substitutional Doping: A first-principles study

## Khushboo Dange, Rachana Yogi, and Alok Shukla\*

Department of Physics, Indian Institute of Technology Bombay, Powai, Mumbai 400076, India E-mail: khushboodange@gmail.com, yogirachana04@gmail.com, shukla@iitb.ac.in

**Abstract.** In this paper we present a thorough first-principles density functional theory based computational study of the structural stability, electronic, magnetic, and optical properties of pristine and doped gallium phosphide (GaP) monolayers. The pristine GaP monolayer is found to have a periodically buckled structure, with an indirect band gap of 2.15 eV. The doping by X (B, Al, In, C, Si, Ge, Sn, Zn, and Cd) at the Ga site, and Y (N, As, Sb, O, S, Se, Te, Zn, and Cd) at the P site is considered, and an indirect to direct band gap transition is observed after doping by In at the Ga site. For several cases, significant changes in the band gap are seen after doping, while the system becomes metallic when O is substituted at the P site. The spin-polarized band structures are calculated for the monolayers with doping-induced magnetism, and we find that for some cases a direct band gap appears for one of the spin orientations. For such cases, we investigate the intriguing possibility of spin-dependent optical properties. Furthermore, for several cases the band gap is very small for one of the spin orientations, suggesting the possibility of engineering half metallicity by doping. For the layers with direct band gaps, the calculated optical absorption spectra are found to span a wide energy range in the visible and ultraviolet regions. The computed formation energies of both the pristine and doped structures are quite small, indicating that the laboratory realization of such structures is quite feasible. On the whole, our results suggest that the doped GaP monolayer is a material with potentially a wide range of applications in nanoelectronics, spintronics, optoelectronics, solar cells, etc.

**Keywords:** Gallium phosphide (GaP) monolayer; band gap engineering; DFT; binding energy; formation energy; magnetism; electronic and optical properties

#### 1. Introduction

In the last couple of decades, with the rapid advances in technology, nano-scaled systems have become the most intensively studied materials [1, 2]. The successful synthesis of graphene [3, 4] with its exclusive properties such as high carrier mobility, good physical strength, 97.2 % transparency, high surface to volume ratio [5, 6, 7], etc., have enthused the research in the field of 2D materials [8, 9, 10, 11, 12]. Synthesis of 2D materials by the techniques such as electrochemical exfoliation [13, 14], chemical vapor deposition [15, 16], etc. is taking place at a rapid rate. 2D materials synthesized till date possess unique electronic, optical, chemical, magnetic, electrical and mechanical properties [17, 18, 19, 20, 21, 22]. They exhibit high carrier mobilities [23, 24], good thermal conductivity [25] and high optical absorption range [26, 27]. Such useful properties make them potential candidates for wide range of applications including batteries [28], energy storage [29], sensors [30], spintronics [31, 32], photodetectors [33], optoelectronics [34, 35], etc.

In particular, binary 2D compounds made up of III-V group elements, have attracted tremendous attention due to their interesting electronic and optical properties, with potentially widespread applications [36, 37, 38, 39, 40, 41, 42, 43, 44]. In spite of such useful properties and applications, 2D compounds that have been synthesized from binary III-V group are limited [45, 46, 47, 48]. Gallium nitride (GaN) monolayer has been synthesized [47] and its properties were explored both experimentally and theoretically. GaN monolayer possesses an indirect band gap of around 2 eV, realized by density functional theory (DFT) calculations [49], which impede its potential for optoelectronic devices [50]. Remarkable efforts have been made to undergo indirect to direct transition by using the strategy of doping [51, 52], adsorption [53, 54], functionalization [55, 56], applying electric field [57] and strain [58, 59]. Similarly, 2D aluminium nitride (AlN) has been synthesized [46] and studied by scientific community [60, 61]. However, some of the III-V monolayers which are predicted [36, 37, 38] to have potential for transformative electronic and optical properties are awaiting discovery.

Bulk Gallium Phosphide (GaP) is an important semiconductor with a wide indirect band gap of 2.26 eV, grown in crystalline form using epitaxial techniques [62, 63]. GaP exhibits interesting properties such as high refractive index, good mechanical durability, spectral transmission range in the infrared region, etc. [64]. These set of properties make GaP a preferable candidate for designing optical elements such as fast lenses, and it opens a route towards visible and near infrared applications [65, 64]. It also plays essential role in high-temperature transistors [66], photovoltaic

solar cells [67], optical devices [68], etc. However in bulk form, modification of electronic and optical properties of any material is possible only up to a certain extent, which can be enhanced further in its reduced dimensional form. As a result, it is important to theoretically study the electronic structure, optical, and magnetic properties of pristine and doped GaP monolayer using a first-principles approach so as to provide some guidance to the experimentalists. GaP thin films were also fabricated using different techniques [69, 70, 71] and were found to have honeycomb like structure similar to silicene [72]. Hexagonal GaP monolayer with slightly buckled honeycomb like structure is predicted to have wide indirect band gap of 2.96 eV computed using HSE06 functional [38], which is higher compared to its bulk counterpart due to quantum confinement effect. Sahin et al. have studied the geometry of III-V monolayers including GaP, along with their electronic and mechanical properties [36]. The GaP monolayer is predicted to be stable in the buckeld form [36]. The dynamic stability of hexagonal GaP monolayer has already been confirmed by the absence of imaginary phonon frequencies [36, 37, 38]. Zhuang et al. used hybrid density functional and the  $G_0W_0$  method to determine the stability and electronic structure of III-V monolayers including GaP. They also demonstrated that GaP monolayer can be synthesized on lattice-matched substrates. Suzuki in 2015 also reported that III-V monolayers are the better candidates for semiconductor devices [38]. A detailed study on the electronic properties of hexagonal GaP monolayer has been reported by Kumar et al. [73] in 2016. Akbari et al. studied the effect of biaxial strain on AlP and GaP monolayers [74], and showed that it is a viable way to tune their electronic as well as optical properties. Facilitating the indirect to direct band gap transition of GaP monolayer using any of the viable way such as doping, functionalization, etc., could be beneficial for its application in the field of optoelectronic devices. Various techniques have been used to tune the electronic properties of nanomaterials such as: passivation [75], adsorption [76], doping [77], defects formation [78], termination [79], functionalization [80] etc. Because doping is much easier and inexpensive to achieve in a laboratory, it is believed to be one of the best ways to tailor the electronic properties of nanomaterials. To the best of our knowledge, the effects of substitutional doping on GaP monolayer have not been reported in the literature till date. Therefore, in this work, we study the effects of substitutional doping on the electronic, magnetic and optical properties of GaP monolayer using a first-principles DFT based methodology.

In this work, we perform a systematic study of the influence of substitutional doping by the same group elements, those from the nearest neighboring groups, and transition metals on the properties of GaP monolayer. In particular, we have studied the structural stability, electronic structure, magnetic, and optical properties of pristine and eighteen substitutionally doped GaP monolayers. We show that for certain dopants, the band gap of GaP monolayer can be tuned from indirect to direct, semiconductor to metallic, and semiconductor to half-metallic. The magnetic

behavior is also observed in certain cases, which is important for spin-dependent transport and optical applications. The variation in Fermi energy also suggests various doping candidates for GaP monolayer. Optical properties of these substitutionally doped GaP monolayer were also investigated, and for several cases spin-dependent optical response was confirmed.

The remainder of this paper is organized as follows. In the next section we briefly discuss our computational approach. Next, in section 3 we present and discuss our results. Finally, in section 4 we present our conclusions and also discuss future prospects.

## 2. Computational Details

All the calculations were performed within the framework of first-principles based DFT [81, 82] using plane wave basis set as implemented in Vienna Ab initio Simulation Package (VASP)[83, 84]. Perdew-Burke-Ernzerhof (PBE) exchange-correlation functional within the generalized gradient approximation (GGA) [85] along with projected augmented wave (PAW) potential [86, 87] was used to solve the Kohn-Sham equations self-consistently. In order to understand the convergence of our calculations with respect to the size of the supercell, we considered three supercells of the GaP monolayer of increasing sizes, namely  $2 \times 2$ ,  $4 \times 4$ , and  $8 \times 8$ , consisting of 8, 32, and 128 atoms, respectively, as discussed in the next section. Subsequently, to balance off the requirements of numerical precision with the computational effort, we performed the rest of our calculations employing the  $4 \times 4$  supercell (see Fig. 1) both for the pristine as well as doped systems. For the doped systems, a single Ga or P atom was substituted by the dopant atom. For the Brillouin zone sampling, Monkhorst-Pack [88] k-point grids of  $5\times5\times1$  and  $7\times7\times1$  were taken for geometry optimization, and self-consistent field (SCF) calculations, respectively. A vacuum space of 12 Å along the z-direction was provided to avoid the interaction between two consecutive layers. The cutoff energy of 500 eV was set for plane wave basis set. The convergence criteria of 10<sup>-5</sup> eV was set to reach the self-consistency. The geometry optimization iterations were continued until the atomic forces on each atom were less than 0.01 eV/Å. Further, a more accurate exchangecorrelation functional, HSE06 [89], is also employed after GGA-PBE [85] to repeat some of the calculations. All the geometry relaxations and SCF calculations were performed within the spinpolarized formalism. Ab initio molecular dynamics (AIMD) [90] simulations are also performed for the doped systems to confirm their stability at high temperatures. For magnetically polarized monolayers, the majority electrons are assumed to have up spin, while minority ones have down spin. For those dopants which were not strongly bound to the monolayer, we also accounted for the van der Waal interactions by including the DFT-D3 [91]. In order to obtain a deeper understanding of the nature of bonding in the systems, we also performed the Bader charge analysis using the

Table 1. Convergence of various parameters with respect to the supercell size.

Supercell	$2 \times 2$	$4 \times 4$	$8 \times 8$
Number of atoms	8	32	128
Lattice constant (Å)	3.85	3.85	3.85
Ga-P bond length (Å)	2.27	2.27	2.27
GaPGa bond angle (degrees)	115.575	115.575	115.575
PGaP bond angle (degrees)	115.573	115.573	115.573
Total Energy per atom (eV)	-4.097	-4.098	-4.106
Binding Energy per atom(eV)	-3.045	-3.045	-3.053

code developed by Henkelman group[92].

#### 3. Results and Discussion

### 3.1. Convergence with respect to the supercell size

The results of our calculations on the pristine monolayer considering supercells of the sizes  $2 \times 2$ ,  $4 \times 4$ , and  $8 \times 8$ , are presented in Table 1. From the table it is obvious that there is perfect agreement among the results obtained using three supercells as far as the geometric parameters such as bond lengths and bond angles are concerned. However, we note small disagreements in the values of: (a) total energy per atom ( $\approx 0.2\%$ ), and (b) binding energy per atom ( $\approx 0.26\%$ ). Because such small disagreements are quite acceptable from a computational point of view, we decided to perform the remainder of our calculations, both on the pristine and doped systems using a  $4 \times 4$  supercell.

## 3.2. Structure and Stability

The optimized structure of pristine GaP monolayer is shown in Fig.1(a) which is a periodically buckled honeycomb like structure similar to that of silicene [72]. In the pristine GaP monolayer, each Ga(P) atom is bonded to three nearest-neighbor P(Ga) atoms. Thus, due to the translational symmetry, all Ga(P) atoms are chemically equivalent to other Ga(P) atoms. We note that for all the three supercells of the pristine monolayer (see Table 1), the optimized lattice constant of 3.85 Å, and the bond angles  $115.575^{\circ}$  ( $\angle$ GaPGa),  $115.573^{\circ}$  ( $\angle$ PGaP) are in close agreement with

the previously reported values [36, 37, 74]. Furthermore, the optimized Ga-P bond length 2.27 Å is also in good agreement with the values reported in the literature [36, 73].

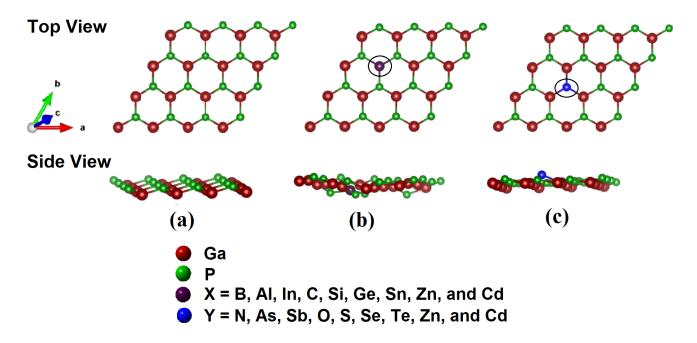


**Figure 1.** Optimized structures of the: (a) pristine GaP monolayer, substitutionally doped GaP monolayers with the dopant at the; (b) Ga site, and (c) P site.

We also present the optimized bond lengths and bond angles of the doped structures computed using the  $4 \times 4$  supercell in Table 2. We note that after doping, the Ga-P bond length varies in the range 2.27-2.41 Å, which signals an average increase. The bond angles  $\angle$ GaPGa and  $\angle$ PGaP undergo more significant changes on doping as compared to the pristine case, with the values in the ranges  $102.85^{\circ}-128.15^{\circ}$ , and  $96.95^{\circ}-128.60^{\circ}$ , respectively. Therefore, it is quite obvious that doping by a single atom has a very significant impact on the structural parameters of the monolayer.

Table 2. The optimized bond lengths and bond angles for the doped structures under investigation.

Bond Le	ength (Å)	e ( degrees)	
Ga(X)P	GaP(Y)	Ga(X)P	GaP(Y)
Ga-P=2.28-2.37	Ga-P=2.27-2.41	$\angle GaPGa = 102.85 - 126.68$	$\angle GaPGa = 103.24-128.15$
P-B = 1.93	Ga-N=1.94	$\angle PGaP = 106.23 - 124.45$	$\angle PGaP = 96.95 \text{-} 128.60$
P-Al=2.33	Ga-As=2.39	$\angle PBP = 117.96$	$\angle GaNGa = 119.97$
P-In=2.47	Ga-O=2.0	$\angle PAlP = 117.33 - 117.35$	$\angle GaAsGa = 104.53$
P-C=1.83	Ga-S=2.31-2.6	$\angle PInP$ =115.10	$\angle GaOGa{=}119.97$
P-Si=2.28	Ga-Se=2.44-2.68	$\angle PCP = 117.50$	$\angle GaSGa = 117.69-119.29$
P-Sn=2.55		$\angle PSiP = 103.29$	$\angle GaSeGa = 113.23 - 115.13$
P-Zn=2.31-2.33		$\angle PSnP = 94.99$	
P-Cd=2.53		$\angle PZnP = 112.07 - 123.37$	
		$\angle PCdP = 116.46 - 121.75$	

To ensure the thermal stability of the pristine structure, the binding energy per atom  $(E_b)$  has been calculated using the relation

$$E_b = \frac{1}{N} \left[ E_{GaP} - (N_{Ga} E_{Ga} + N_P E_P) \right] \tag{1}$$

where  $E_{GaP}$  is the total energy of pristine GaP monolayer,  $E_{Ga}$ , and  $E_P$  are the energies of isolated Ga and P atoms, respectively. Further,  $N_{Ga}$  and  $N_P$  denote the numbers of Ga and P atoms, respectively in the supercell, while  $N = N_{Ga} + N_P$  is the total number of atoms. The resultant binding energy calculated using Eq. 1 is -3.045 eV/atom which confirms that the structure is thermodynamically stable. GaP monolayer is energetically less stable than its 3D bulk counterpart, with a relative energy of 0.45 eV/atom [37]. However, it is less than the relative energy of the 2D hexagonal monolayer of SiC (0.50 eV/atom) which has recently been synthesized [93]. Another important quantity from an experimental point of view is the formation energy ( $E_f$ ) of the pristine GaP monolayer defined as[94]

$$E_f = [E_{GaP} - (N_{Ga}\mu_{Ga} + N_P\mu_P)], \qquad (2)$$

where  $\mu_{Ga}$  and  $\mu_P$ , respectively, represent the chemical potentials of Ga and P corresponding to their most common bulk phases. We performed DFT calculations of the chemical potentials of various elements using the VASP code[84, 83, 86], and the computed values are presented in

Table S1 of the SI (supporting information). Employing those values of chemical potentials, the computed value of the formation energy of the pristine GaP monolayer is rather small at 0.032 eV, indicating that the synthesis of GaP monolayer is chemically feasible. Furthermore, the dynamical stability of the GaP monolayer has been verified by several authors in previous works by computing its phonon spectra, in which no imaginary frequencies were found [36, 37, 38].

Next, we optimized the geometries of the substitutionally doped GaP monolayers, and the results are presented in Fig.1(b),(c). We denote the doped structures as Ga(X)P and GaP(Y), where X(=B, Al, In, C, Si, Ge, Sn, Zn and Cd) and Y(=N, As, Sb, O, S, Se, Te, Zn, and Cd) are the dopants replacing Ga and P atoms, respectively. Of all the optimized structures obtained by substituting the Ga atom, we note that the Ge-doped structure results in the physisorption of the dopant atom, whereas all other dopants are involved in chemical bond formation with their nearest neighbor host atoms. Similarly, in case of the substitution of P atom, we note that Sb, Te, Zn, and Cd doping resulted in physisorption, whereas other dopants are involved in chemical bond formation with the host atoms. For the doped GaP monolayers which exhibit physisorption, we have performed DFT-D3 calculations using Grimme dispersion correction method [91] to account for the van der Waal contribution to the binding energy. However, we found that in all the cases of physisorption, the contribution of the Grimme correction to the total energy was insignificant (less than  $1.0 \times 10^{-6}$  eV), except for Ga(Ge)P for which it was 5.5 meV and has been included in the binding energy reported in Table 3. To verify the structural stability, first we have calculated the binding energies of all the optimized structures obtained by doping impurity elements in GaP monolayer. The binding energies per atom for the doped systems,  $E_b^{(d)}$ , are calculated by using the expression

$$E_b^{(d)} = \frac{1}{N} \left[ E_{tot} - \left( N_{Ga} E_{Ga} + N_P E_P + E_{X/Y} \right) \right]$$
 (3)

where  $E_{tot}$  is the total energy of doped GaP monolayer,  $E_{Ga}$ ,  $E_P$ , and  $E_{X/Y}$  respectively, represent the total energies of the isolated Ga, P, and dopant atoms, and  $N_{Ga}$ ,  $N_P$ , denotes the number of Ga, P atoms in the doped system, respectively, with  $N = N_{Ga} + N_P + 1$ . The obtained values of  $E_b^{(d)}$  along with the binding energy relative to that of the pristine monolayer,  $\Delta E_b^{(d)} = E_b^{(d)} - E_b$  for Ga and P substituted cases are presented in Tables 3 and 4, respectively. We note that the binding energy per atom for the doped systems in most of the cases is lower than that of the pristine system, as also indicated by the negative sign of the relative binding energy  $\Delta E_b^{(d)}$  in those cases, suggesting higher stability as compared to the pristine monolayer. The magnitudes of the relative binding energies  $\Delta E_b^{(d)}$  for these systems are in the range 5 meV – 140 meV, indicating their thermodynamic stability and practical realization. However, opposite is the case for doping with the transition metals Zn and Cd in place of both Ga and P, and also

for doping with As and Te in place of P for which  $\Delta E_b^{(d)} > 0$ , indicating instability of the lattice, possibly due to the large ionic radii of the dopant atoms. This suggests that for these cases the resulting lattice will be highly strained. We also computed the formation energies for the doped systems,  $E_f^{(d)}$ , using the expression [95]

$$E_f^{(d)} = \left[ E_{tot} - (E_{GaP} - \mu_{Ga/P} + \mu_{X/Y}) \right], \tag{4}$$

where  $\mu_{Ga/P}$  and  $\mu_{X/Y}$  denotes the chemical potential of a Ga/P atom removed and considered doping element X/Y, respectively. The resultant formation energies  $(E_f^{(d)})$  computed using the values of the chemical potentials listed in Table S1 of the SI are presented in Tables 3 and 4 for the Ga and P substituted cases, respectively. The negative formation energies obtained for all the doped cases except Ga(C)P, GaP(As), GaP(Zn), and GaP(Cd) systems suggests that the formation of these substitutional doped GaP monolayer is practically feasible, and the doped monolayers will be more stable as compared to their pristine counterpart. Further, the small positive values of  $E_f^{(d)}$  for Ga(C)P, GaP(As), GaP(Zn), and GaP(Cd) systems are favorable according to the literature [96] and thus the practical realization of these doped GaP layers is also possible.

**Table 3.** The calculated binding energy  $(E_b^{(d)})$ , relative binding energy  $(\Delta E_b^{(d)})$ , formation energy  $(E_f^{(d)})$ , magnetic moment  $(\mu, \text{ in Bohr magnetons})$ , Fermi energy  $(E_F)$ , and electronic band gap  $(E_g)$  of all the structures obtained by the substitutional doping of pristine GaP monolayer in place of Ga atom (Ga(X)P).

Configurations	$E_b^{(d)}$ (eV)	$\Delta E_b^{(d)}$ (eV)	$E_f^{(d)}(eV)$	$\mu$	$E_F(eV)$	$E_g(eV)$		
		$\Sigma_{\Gamma}(\circ \cdot)$	majority spin	minority spin				
GaP (pristine)	-3.045	0.000	0.032	0.00	-3.06	2.15 I		
Ga(B)P	-3.185	-0.140	-0.782	0.00	-3.19	1.81 I		
Ga(Al)P	-3.116	-0.071	-1.451	0.00	-3.14	2.00 I		
Ga(In)P	-3.050	-0.005	-0.576	0.00	-3.12	2.00 D		
Ga(C)P	-3.164	-0.119	1.437	0.52	-2.00	0.64 I	1.25 I	
Ga(Si)P	-3.117	-0.072	-0.402	0.42	-2.26	1.21 I	1.57 D	
Ga(Ge)P	-3.095	-0.050	-0.432	0.49	-2.52	1.45 I	1.11 D	
Ga(Sn)P	-3.072	-0.027	-0.424	0.55	-2.65	1.50 I	0.85 D	
Ga(Zn)P	-3.016	0.029	-0.685	0.44	-3.24	2.21 I	0.21 D	
Ga(Cd)P	-2.995	0.050	-0.416	0.46	-3.26	2.12 D	0.12 D	

 $\overline{I} \equiv \text{Indirect gap and } D \equiv \text{Direct gap}$ 

**Table 4.** The calculated binding energy  $(E_b^{(d)})$ , relative binding energy  $(\Delta E_b^{(d)})$ , formation energy  $(E_f^{(d)})$ , magnetic moment  $(\mu, \text{ in Bohr magnetons})$ , Fermi energy  $(E_F)$ , and electronic band gap  $(E_g)$  of all the structures obtained by the substitutional doping of pristine GaP monolayer in place of P atom (GaP(Y)).

Configurations	$E_b^{(d)}(\text{eV})  \Delta E_b^{(d)} \text{ (eV)}  E_f^{(d)}(\text{eV})  \mu  E_F$	$\Delta E^{(d)}$ (eV)	$E^{(d)}(eV)$	11	$E_F(eV)$	$E_g(eV)$		
		$\mathcal{L}_{F}(\mathfrak{s},\mathfrak{t})$	majority spin	minority spin				
GaP(N)	-3.131	-0.086	-1.027	0.00	-3.14	1.64 I		
GaP(As)	-3.023	0.022	0.912	0.00	-3.06	$2.07 \; {\rm I}$		
GaP(Sb)	-3.059	-0.014	-1.353	0.00	-3.26	2.13 I		
GaP(O)	-3.130	-0.085	-2.828	0.00	-3.19	M		
GaP(S)	-3.085	-0.040	-1.545	0.54	-2.01	0.99 I	1.71 D	
GaP(Se)	-3.057	-0.012	-1.172	0.55	-2.52	0.88 I	1.21 D	
GaP(Te)	-3.029	0.016	-0.492	0.54	-3.12	1.09 I	1.44 D	
GaP(Zn)	-2.941	0.104	0.934	0.60	-2.58	0.96 D	0.23 I	
GaP(Cd)	-2.938	0.107	0.606	0.55	-2.51	0.88 D	0.13 I	

 $I \equiv Indirect$ ,  $M \equiv Metallic$ , and  $D \equiv Direct$ 

Further, we have also performed the AIMD [90] calculations for all the doped GaP monolayers. These simulations are useful for validating the stability of systems at high temperatures [97, 98, 99], and were performed in the canonical ensemble for 5 ps with a time step of 1 fs at a constant temperature of 500K by using the Nose-Hoover thermostat [100]. The total energy of all the doped systems is plotted as a function of time steps for all the considered systems (see SI), while the results for Ga(Ge)P and GaP(Te) systems are presented in Fig. 2. We note that the total average energy remains constant in spite of slight variation in energies with time. The corresponding geometries remain stable at 500K as shown in the inset. The changes in Ga-P bond lengths are 0.09 Å and 0.06 Å for the Ga(Ge)P and GaP(Te) systems, respectively, whereas the change in P-Ge and Ga-Te bond lengths are 0.07 Å and 0.007 Å, respectively. The results of AIMD simulations for the rest of the doped cases show similar behavior as depicted in Figs. S1 and S2 of the SI. These findings suggests that all the doped GaP monolayers are thermodynamically stable at high temperatures.

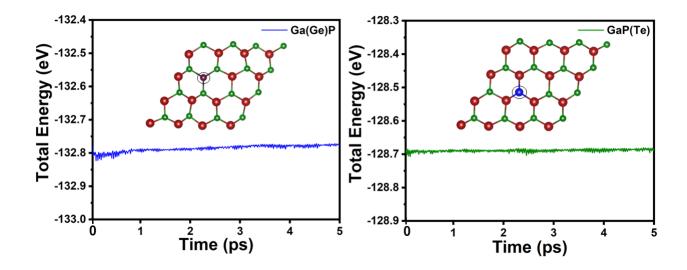


**Figure 2.** The variations of the total energy of (a) Ga(Ge)P and (b) GaP(Te) monolayers with time at 500K. Corresponding geometries are shown in inset.

#### 3.3. Electronic Structure

3.3.1. Pristine Monolayer In order to check the convergence of the band structure with respect to the supercell size, we computed the electronic band structures of the  $2 \times 2$ ,  $4 \times 4$ , and  $8 \times 8$  supercells of pristine GaP monolayer using GGA-PBE [85] functional as illustrated in Fig. 3. From the figure it is obvious that except for the total number of bands, the band structure for the three supercells are virtually identical. In all the three cases, the valence band maximum (VBM) and conduction band minimum (CBM) are located at K and  $\Gamma$  points, respectively, with an indirect band gap of 2.15 eV, in agreement with the values reported in literature for the  $2 \times 2$  and  $4 \times 4$  supercells [38, 73]. Since the band structures computed for the three supercells show a similar trends, we have continued our investigation of pristine and doped monolayers using the  $4 \times 4$  supercell.

We present the band structure, density of states (DOS), and atom projected density of states (PDOS) of the pristine  $4 \times 4$  GaP monolayer, computed using GGA-PBE [85] functional in Fig.4. To further probe the electronic structure, we calculated the corresponding DOS (Fig. 4(b)) which shows good agreement with the band structure. Given the mirror symmetry between up- and downspins in the DOS plot, it is obvious that the pristine GaP monolayer is non-magnetic in nature. To understand the atomic contributions to the electronic structure of the pristine GaP monolayer, we present its PDOS in Fig. 4(c) from which it is obvious that the valence band derives more

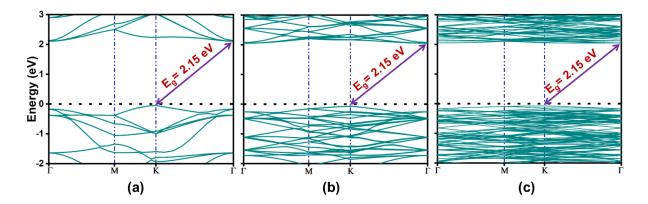


**Figure 3.** Calculated electronic band structures of (a)  $2\times2$ , (b)  $4\times4$ , and (c)  $8\times8$  GaP monolayers using GGA-PBE functional.

contributions from the P-based orbitals, while the conduction band is dominated by Ga orbitals. The band structure of the pristine  $4 \times 4$  GaP monolayer is also calculated using hybrid exchange correlation functional, HSE06 [89], and is presented in Fig. 5. The calculated band structure also predicts an indirect band gap  $(K \to \Gamma)$  with the nature of energy states identical to that of the GGA-PBE counterpart (Fig. 3(a)). However, as expected, the band gap gets increases to 2.94 eV which shows excellent agreement with the previously reported value [38].

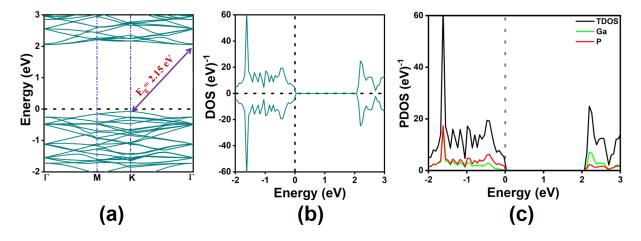


**Figure 4.** (a) Electronic band structure, (b) Density of states (DOS), and (c) projected density of states (PDOS) of the pristine GaP monolayer using GGA-PBE [85] functional. Black dotted line represents the Fermi level ( $E_F$ ) which is set at 0.00 eV.

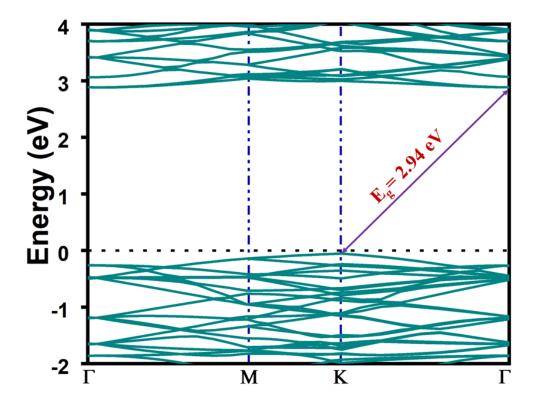


**Figure 5.** Electronic band structure of the pristine GaP monolayer using HSE06 functional. Black dotted line represents the Fermi level  $(E_F)$  which is set at 0.00 eV.

3.3.2. Doped monolayers: Induced Magnetism Next, we investigate the influence of substitutional impurities on the properties of the GaP monolayer. Recently, there have been several studies of the induced magnetism in non-magnetic materials by impurity doping in order to investigate their potential for magnetic applications [101, 102]. Therefore, we also decided to investigate the magnetic properties of the doped GaP monolayers by performing spin-polarized calculations and computing the magnetic moments, the results of which are presented in Tables 3 and 4. We note that there is a significant amount of nonzero magnetic moment in the supercell when a single Ga is replaced by a group IV element, or by transition metal (TM) atom Zn/Cd. In fact, the maximum induced moment is for Sn doping. For the case of P substitution (Table 4), we obtain finite magnetic moments for chalcogens (except O) and TM doping, with the maximum moment obtained for Zn doping. To determine the nature of the induced magnetism, we have performed spin polarized calculations corresponding to ferromagnetic (FM) and antiferromagnetic (AFM) configurations for

each such monolayer. For these calculations, we have used the extended supercell of size  $8 \times 4 \times 1$ , as discussed in the literature [95, 96]. The energy difference between the FM and AFM states is calculated as  $\Delta E = E_{FM} - E_{AFM}$  and presented in Table 5. According to this definition of  $\Delta E$ , its negative (positive) value suggests the stability of the corresponding doped GaP monolayer in the FM (AFM) state. Consequently, it is clear from the obtained values of  $\Delta E$  that Ga(C)P, Ga(Ge)P, and GaP(Cd) structures are stable, in the FM state, whereas the other ones are in the AFM state.

**Table 5.** Calculated energy difference ( $\Delta E$ ) between the FM and AFM states for the magnetism induced structures in case of both the Ga and P-substituted monolayers.

Systems	Ga-substituted monolayers								
	Ga(C)P	Ga(Si)P	Ga(Ge)P	Ga(Sn)P	Ga(Zn)P	Ga(Cd)P			
$\Delta E \text{ (eV)}$	-1.33	0.004	-0.004	0.003	0.004	0.005			
Systems		P-substituted monolayers							
	GaP(S)	GaP(Se)	GaP(Te)	GaP(Zn)	GaP(Cd)				
$\Delta E \text{ (eV)}$	0.0004	0.0009	0.0007	0.013	-3.405				

To further study the induced magnetism, we have computed the spin density differences, and plotted them in Figs. 6 and 7, for the Ga- and P-substituted systems, respectively. For the Ga-substituted systems, we note that except for the TM doped monolayers, major contribution to the induced magnetism comes from the dopant and nearby atoms (Figs. 6(a),(b),(c),(d)). However, for the Zn and Cd doped monolayers, their nearest neighbor elements are responsible for the induced magnetism (Figs.6(e),(f)). From Fig.7, it is obvious that for P-substituted systems, the dominant contribution to the magnetic moment is from the atoms near to the doped site.

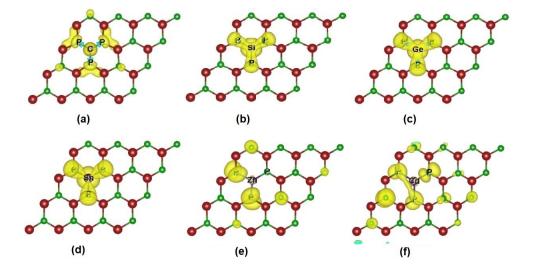


**Figure 6.** Spin density difference plots for Ga-substituted monolayers: (a) Ga(C)P, (b) Ga(Si)P, (c) Ga(Ge)P, (d) Ga(Sn)P, (e) Ga(Zn)P, and (f) Ga(Cd)P. Here yellow and blue colors represent the majority and minority spin densities, respectively.

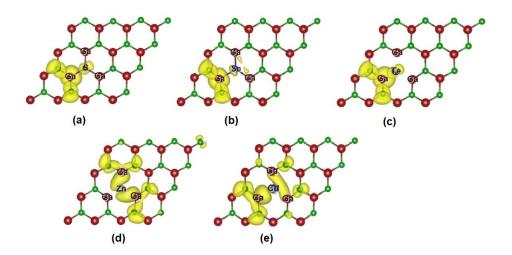


**Figure 7.** Spin density difference plots for P-substituted monolayers: (a) GaP(S), (b) GaP(Se), (c) GaP(Te), (d) GaP(Zn), and (e) GaP(Cd). Yellow and blue colors represent the majority and minority spin densities, respectively.

Next, we will discuss the calculated spin-polarized electronic band structures for these magnetic systems, and electronic band structures for other impurities doped GaP monolayer which

remains non-magnetic.

Band Structure of Ga-substituted monolayers First, we discuss the band structures of substitutionally doped GaP monolayers with one Ga atom of the supercell replaced by group III elements, namely, B, Al and In. In Fig. 8 we present the band structure and DOS of Ga(In)P, while in Fig. S3 of the SI, corresponding plots for Ga(B)P and Ga(Al)P are presented. The band gaps for all the monolayers are listed in Table 3. When compared to the pristine case, we note that for all the three doped cases, a prominent impurity band (IB) appears just below the lowest conduction band in the gap region. This leads to a lowering of the electronic band gap to 1.81 eV, 2.00 eV, and 2.00 eV for B, Al, and In dopants, respectively. We consider this lowering to be significant in light of the fact that the doping percentage is only 6.25. As far as the nature of the band gap is concerned, it remains indirect for B- and Al-doped monolayers, however, for the In-doped case, the band gap transforms quite interestingly into a direct one at the  $\Gamma$  point. This implies that in Ga(In)P, optical transitions are possible across the gap, which clearly has important technological implications for the design of GaP monolayer based optoelectronic devices. In addition to the IB near the conduction band, several new bands appear near the top of the valence band, thereby increasing the DOS in that region, which is obvious from the DOS plots of Figs. 8 and S3. The PDOS for the three doped monolayers is plotted in Fig. S4 of the SI. As far as the contribution of Ga and P atoms to the PDOS is concerned, the trends are unchanged as compared to the pristine monolayer, with P contributing more to the valence bands, while Ga contributing more to the conduction bands. As far as the impurity atoms are concerned, predictably their contributions are small and concentrated near the Fermi energy  $E_F$ .

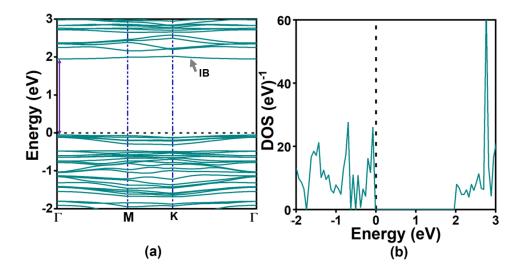


**Figure 8.** (a) Band structure, and (b) DOS plots for the Ga(In)P structure. The impurity band (IB) is indicated by an arrow.

The spin-polarized electronic band structures are calculated for those Ga-substituted cases which resulted in nonzero magnetic moments discussed in the previous section. In Fig. 9 we present the calculated spin-polarized band structures for Ga(C)P and Ga(Zn)P systems from which the splitting of energy states corresponding to charge carriers of majority (green) and minority (red) spins is obvious. The nature of band gap remains indirect corresponding to both the spin carriers for Ga(C)P system (Fig.9(a)), whereas it becomes direct for minority spin carriers when doped with  $\operatorname{Zn}$  (Fig.9(c)). This suggests the interesting possibility of spin-dependent optical transitions across the direct bang gaps. It is worth mentioning that the impurity doping resulted in additional energy states. However, unlike the non-magnetic cases (B, Al, and In doping), large number of additional energy states (ranging from 1.6 eV to 2 eV) get induced in the forbidden energy region due to doping of C atom as it plays a role of donor impurity. Also, these induced energy states corresponds to the charge carriers of both the majority and minority spins. This is also confirmed by the corresponding DOS presented in the same figure (Fig.9(b)) which shows the emergence of peaks in this particular region. Also, the asymmteric DOS profile corresponding to two spin orientations verifies the induced magnetism in these doped monolayers. Additionally, it is quite interesting to observe that one of the impurity energy states which splits into majority and minority charge carriers appeared near the Fermi energy level (indicated by arrow). Similar trend is also observed in the electronic band structure of Ga(Si)P, Ga(Ge)P, Ga(Sn)P, and Ga(Cd)P systems shown in Fig. S5 of the SI. The corresponding DOS presented in the same figure shows good agreement with their band structures. The magnitude as well as nature of the resultant band gap are discussed in Table 3. Unlike other magnetism induced cases, the band gap becomes direct for the charge carriers of both spin orientations for the Ga(Cd)P system. Another noteworthy point is the significant difference between the band gaps of majority and minority spin carriers for the doped monolayers Ga(C)P, Ga(Sn)P, Ga(Zn)P, and Ga(Cd)P. In particular for Ga(Zn)P, and Ga(Cd)P, the minority carrier band gap almost closes, i.e., they are almost half-metallic, suggesting their possible applications in spintronic devices. From the PDOS shown in Fig. S6 of the SI, we can conclude that similar to the pristine monolayer, the maximum contribution in valence band comes from the valence orbital of P, whereas valence orbital of Ga contributes significantly to the conduction band. Dopant atom contributes to the states near  $E_F$  where the impurity bands are located.

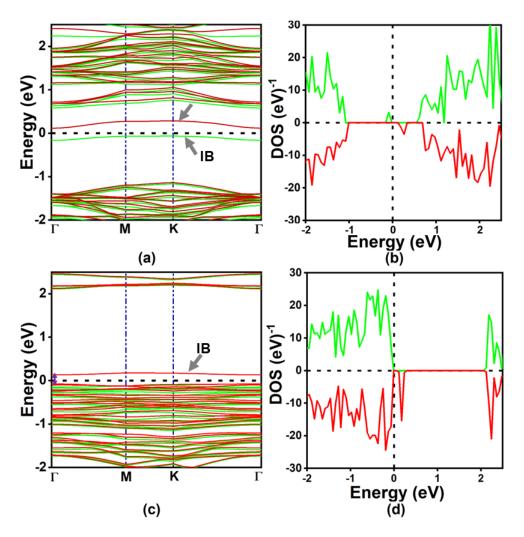


**Figure 9.** (a) and (b) band structure and DOS, respectively, for Ga(C)P, (c) and (d) band structure and DOS, respectively, for Ga(Zn)P structures. Green and red lines represent energy states corresponding to majority and minority spin electrons, respectively. Impurity bands (IB) are indicated by arrows.

The band structure is also calculated using the HSE06 functional only for one of the Gareplaced cases, i.e, Ga(C)P, due to the high computational costs of such calculations, and the results are presented in Fig. 10. The HSE06 functional increased the  $E_g$  corresponding to both the majority and minority spin carriers to 2.44 eV and 1.96 eV from the earlier values of 0.64 eV and 1.25 eV, respectively, obtained using PBE functional. The nature of the bands remains the same and therefore the nature of the gap remains indirect for both the spin carriers.

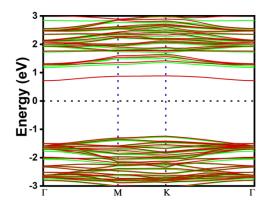


**Figure 10.** The electronic band structure of the Ga(C)P structure calculated using the HSE06 functional. The green and red lines represent the bands corresponding to majority and minority spin electrons, respectively. Black dotted line represents the Fermi level  $(E_F)$  which is set at 0.00 eV.

Substitutional doping by different impurity elements also leads to changes in the Fermi energy  $(E_F)$  as compared to that of the pristine GaP monolayer. It is observed from Table 3, that  $E_F$  in case of doping with the same group elements shifts towards the valence band thus showing a p-type behavior. Similar behavior is observed for TM impurities (Zn/Cd) and the reason is that substitutional doping by these elements in place of the Ga atom leads to their bond formation with a P atom. But, Ga has three valence electrons whereas, the TM atom contains only two valence electrons, thus resulting in deficiency of one electron in forming a bond with P atom as compared to the pristine Ga-P bond, leading to hole formation, i.e., p-type doping. However, doping by group IV elements resulted in upward shift (towards the conduction band) in  $E_F$  because of one extra electron than in their outer shell as compared to the Ga atom, thereby effectively leading to n-type doping.

3.3.4. Band Structure of P-substituted monolayers Next, we discuss the results of our calculations on the P-substituted monolayers of the type GaP(Y). As discussed earlier, for Y=N, As, Sb and O, our calculations predict non-magnetic ground states. The calculated band structures of N and O-doped GaP monolayers are presented in Fig. 11, from which it is obvious that a single impurity band gets formed around 1.5 eV in the gap region, for the N-doped monolayer. Due to this, the magnitude of the band gap reduces significantly to 1.64 eV, with still an indirect band

gap. However, a drastic change is observed for the GaP(O) system which turns metallic due to the dopant O atom, which may be useful from a device perspective [103]. All these modifications in the band structure after N and O doping are validated by the corresponding DOS plots of Figs. 11(b) and 11(d), respectively. The electronic band structure and corresponding DOS for GaP(As) and GaP(Sb) structures are plotted in Fig. S7 of the SI. The variations in the band gaps as a function of doping elements are presented in Table 4. We note that the As and Sb impurities changed the band gap of GaP monolayer very slightly to 2.07 eV and 2.13 eV, respectively, while retaining the indirect nature of the gap. In Fig. S8 of the SI we plot the PDOS for all the four dopants (N, As, Sb and O). We note that the contributions of P and Ga atoms to PDOS near  $E_F$  exhibit the same trends as for the pristine monolayer. However, the dopant atom contributes to the PDOS near  $E_F$  only for Sb doping. For other monolayers, it contributes to states further away from  $E_F$ . For the O-doped monolayer, the states at  $E_F$  leading to its metallic nature are derived predominantly from the P and Ga atoms.

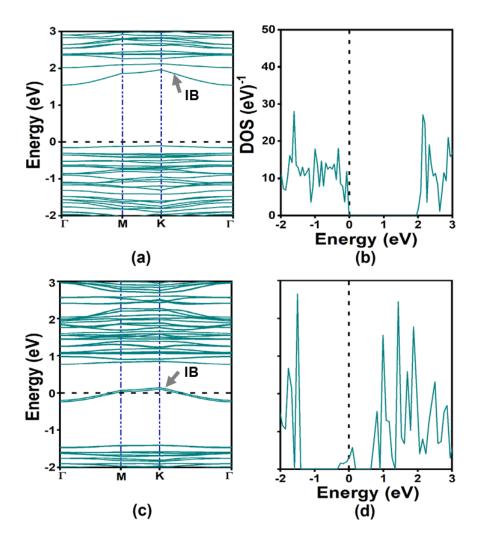


**Figure 11.** Electronic band structure/DOS plots for (a)/(b) GaP(N), and (c)/(d) GaP(O) monolayers. The impurity bands (IB) are indicated by arrows.

The spin-polarized electronic band structures are calculated for the P-substituted GaP monolayer with chalcogens (S, Se, and Te) and TM (Zn/Cd) as the dopants. The electronic band structures and corresponding DOS for two representative monolayers GaP(S) and GaP(Zn) are presented in Fig.12. We note that some additional bands, which are quite flat, have appeared near the Fermi level corresponding to the charge carriers of both the spins, denoted as IB in the figure. In addition to the IBs close to  $E_F$ , some other IBs also emerge which are somewhat farther from the Fermi level. Transition from the indirect to a direct band gap is observed for minority (majority) spin electrons for doping with S (Zn) atoms. The spin-polarized electronic

band structures and corresponding DOS for Se, Te, and Cd doped cases are shown in Fig. S9 of the SI. The direct (indirect) band gap is observed for the minority (majority) spin electrons both for Se and Te doping, similar to the case of GaP(S) monolayer. Whereas, opposite behavior is observed for Cd doping, with the majority band gap becoming direct, just as in the case of the GaP(Zn) layer. Again, the asymmetric nature of DOS in all the cases corresponding to majority and minority spin electrons is consistent with the induced magnetism. The magnitude of resultant band gaps for all the cases are presented in Table 4 from which again a strong tendency towards half metallicity is obvious for TM (Zn, Cd) doped GaP monolayers. The calculated PDOS (Fig. S10 of the SI) for induced magnetism cases shows that again the maximum contribution in the valence and the conduction bands comes from the valence orbitals of P and Ga atoms, respectively, with important contributions by the dopant atoms to the impurity bands near  $E_F$ .

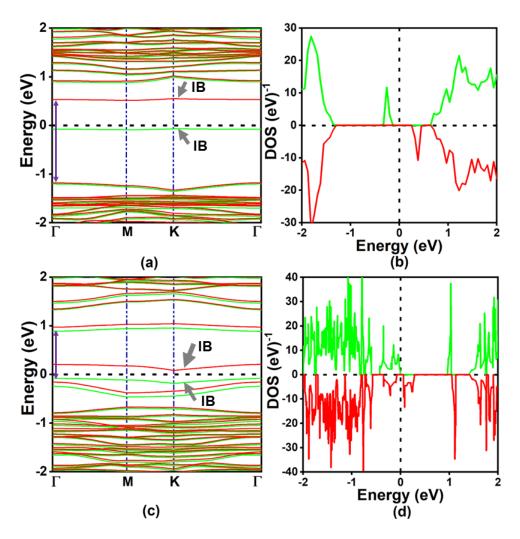


**Figure 12.** Electronic band structure/DOS for (a)/(b) GaP(S), and (c)/(d) GaP(Zn) systems. Here green and red color lines represent energy states corresponding to majority and minority spin charge carriers respectively. Impurity bands (IB) are indiacted by arrow.

Next, we present the HSE06 band structures for the two P-replaced cases, i.e., GaP(N) and GaP(Zn), in Fig. 13, and note that while the GaP(N) monolayer remains nonmagnetic, the GaP(Zn) monolayer becomes magnetic, in agreement with the PBE results. Expectedly, the band gaps get increased to 2.55 eV for the GaP(N) system, and to 1.6 eV (0.48 eV) corresponding to majority (minority) spin carriers of the GaP(Zn) system. However, the nature of the bands and the band gaps remain identical to those obtained using PBE functional, i.e. indirect for GaP(N) system, whereas, direct (indirect) for GaP(Zn) system corresponding to majority (minority) spins.

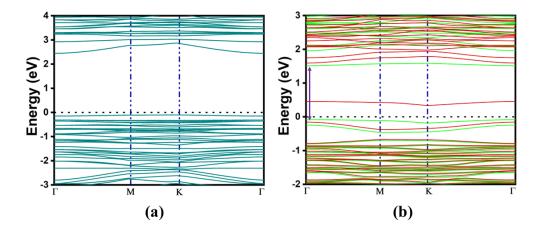


Figure 13. The electronic band structures of the (a) GaP(N) and (b) GaP(Zn) monolayers calculated using the HSE06 functional. The green and red lines represent the bands corresponding to majority and minority spin electrons, respectively. Black dotted line represents the Fermi level  $(E_F)$  which is set at 0.00 eV.

The variation in  $E_F$  as a function of dopant elements, as presented in Table 4, also shows interesting behavior. The doping of N, Sb, O, and Te impurities shifted the  $E_F$  towards the valence band leading to effectively p-type doping as compared to the pristine counterpart, whereas for S, Se, Zn and Cd doping, it shifted towards the conduction band leading to n-type doping. However, the  $E_F$  remains unchanged in case of As doped GaP monolayer.

3.3.5. Bader charge analysis To investigate the influence of doping on the charge distribution in the monolayers, we have performed the Bader charge analysis, and the results are presented in Table 6. In the table we present the Bader charges on the doping site (Ga/P), and its three nearest-neighbor atoms (P/Ga) before and after the doping. We note that in all the cases of doping at the Ga site (except for C doping), the charge gets transfered from the dopant to the nearest neighboring P atoms due to the relatively higher electronegativity of P atoms than the dopants. However, the opposite result is observed for C doping because P atom is less electronegative as compared to the C atom. For the cases of P-site substitution, it is observed that the dopants (except Zn and Cd) gain charge from its nearest atoms (Ga), the reason for which can again be explained in terms of electronegativity differences, i.e., dopants are more electronegative than the Ga atom. In case of TM doping, we get an interesting result that both the dopant and Ga atoms lose charge because of their comparable electronegativities. As a result, the charges from the dopant (Zn and Cd) and Ga atoms get transferred to the nearest P atoms, which are more electronegative as compared to them.

**Table 6.** Charge accumulated on dopant and its nearest neighbor atoms for both the Ga and P substituted structures, i.e. Ga(X)P and GaP(Y).

Accumulated charge (e)									
	$\overline{\text{Ga}(X)P}$				GaP(Y)				
Dopant	P1	P2	Р3	Dopant	Ga1	Ga2	Ga3		
Ga=2.26	5.73	5.73	5.73	P=5.73	2.26	2.26	2.26		
B=2.54	5.67	5.67	5.66	N=5.98	2.32	2.32	2.32		
Al=1.10	6.12	6.12	6.12	As=5.49	2.32	2.32	2.32		
In=2.29	5.69	5.69	5.69	Sb = 5.25	2.41	2.41	2.41		
C=5.35	4.98	4.98	4.96	O=7.11	2.11	2.11	2.11		
Si=2.84	5.85	5.85	5.84	S=6.82	2.44	2.17	2.17		
Ge=3.46	5.66	5.66	5.66	Se=6.66	2.46	2.23	2.23		
Sn=3.30	5.70	5.70	5.70	Te=6.39	2.50	2.32	2.32		
Zn=11.41	5.68	5.68	5.70	Zn=11.89	2.54	2.54	2.51		
Cd=11.44	5.68	5.68	5.65	Cd=11.90	2.50	2.50	2.50		

#### 3.4. Optical Properties

We saw in the previous section that for several cases of doping band gap becomes direct, implying that those systems could be useful in optoelectronic devices. Also in some cases a direct band gap is only observed for electron's one spin orientation, implying spin-dependent optoelectronic properties. Therefore, we decided to compute optical absorption spectra of the studied monolayers, both for the pristine and doped ones. For the purpose, we have calculated the dielectric functions, refractive indices, and absorption coefficients for the layers with a direct band gap after doping. The information regarding the response of a material to an incident external electromagnetic radiation of frequency  $\omega$  is contained in the dielectric function  $\varepsilon(\omega) = \varepsilon_1(\omega) + i\varepsilon_2(\omega)$ , where  $\varepsilon_1(\omega)$  and  $\varepsilon_2(\omega)$ are its real and imaginary parts, respectively. The imaginary part of dielectric function is calculated by taking summation of the conduction band states, while its real part is obtained by applying the Kramers-Kronig relationship. Our calculations of the optical absorption spectra were within the framework of the independent particle model (IPM) in which only band-to-band electronic transitions are considered. That is, the influence of electron (e) -hole (h) interactions was neglected which give rise to the formation of midgap excitons. To incorporate the e-h interactions, one needs to employ methodologies like Bethe-Salpeter equation (BSE) [104, 97, 98, 105, 106], which go beyond IPM and include quantum many-body effects. Nonetheless, the main objective of these calculations is to attain a qualitative grasp of how defects change the optical properties of the GaP monolayer, for which we feel that IPM suffices. However, for a quantitatively accurate description of the optical properties of the GaP monolayer, computationally demanding BSE approach will be necessary. The refractive index  $n(\omega)$ , and absorption coefficient  $\alpha(\omega)$  are also calculated using the equations

$$n(\omega) = \frac{1}{\sqrt{2}} \left[ \sqrt{\epsilon_1^2(\omega) + \epsilon_2^2(\omega)} + \epsilon_1(\omega) \right]^{\frac{1}{2}}$$
 (5)

$$\alpha(\omega) = \frac{\omega\sqrt{2}}{c} \left[ \sqrt{\epsilon_1^2(\omega) + \epsilon_2^2(\omega)} - \epsilon_1(\omega) \right]^{\frac{1}{2}}$$
(6)

The real and imaginary parts of the dielectric function are plotted for both Ga(X)P (Ga substitution) and GaP(Y) (P substitution) structures in Fig. 14. The imaginary part of the dielectric function experiences a red shift after doping in all the considered cases (see Figs. 14(b),(d)) due to the doping-induced band gap reduction. The real part of the dielectric function increases for the doped monolayers as compared to the pristine one (see Figs. 14(a),(c)). The high value of dielectric constant reduces the amount of radiative recombination, consequently enhances the device performance as far as solar cells are concerned [107, 108].

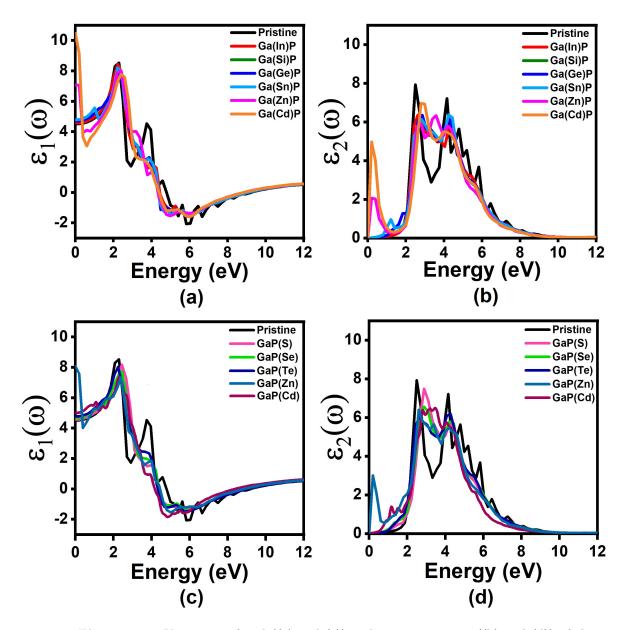


**Figure 14.** Variations of real ((a) and (c)) and imaginary parts ((b) and (d)) of the complex dielectric functions, respectively for the Ga(X)P and GaP(Y) systems, with respect to the energy of the incident light.

The refractive indices  $n(\omega)$  calculated using Eq. 5 are presented in Fig. S11 of SI. Further, we have also calculated the optical absorption coefficients  $\alpha(\omega)$  (using Eq. 6) for the pristine and

those doped GaP monolayers with direct band gaps for at least one spin orientation, and compared them to that of the pristine monolayer.

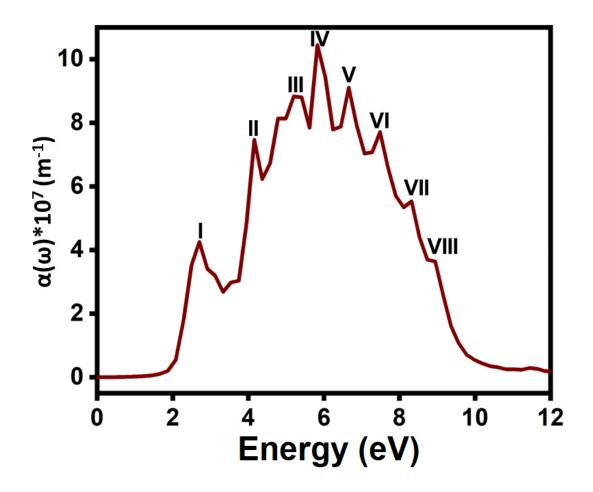


Figure 15. Optical absorption coefficient  $\alpha(\omega)$  of the pristine GaP monolayer as a function of the energy of the incident photon.

In Fig. 15 we plot the absorption coefficient  $(\alpha(\omega))$  of the pristine GaP monolayer, which is fairly broad spanning the energy region 2.0 eV – 10.0 eV. Nevertheless, the spectrum has several well-defined peaks which are labeled in the figure, and whose positions are listed in Table 7. Because the pristine monolayer is an indirect band gap material, the peaks in its absorption spectrum are located at energies higher than the band gap of 2.15 eV. The first peak occurs at 2.70 eV corresponding to the transition  $v \to c+5$ , at the K point, where v/c denote the highest/lowest

valence/conduction band. Similarly, the maximum intensity peak IV, located at 5.82 eV is due to the transition  $v \to c + 34$ , at the  $\Gamma$  point. The full list of transitions corresponding to various peaks of the absorption spectra is presented in Table S2 of the SI from which it is obvious that the absorption peaks at successively higher energies involve transitions from the highest valence band into the high-lying conduction bands. However, noteworthy point is that the spectra are calculated within the mean-field approximation of DFT, and, thus do not include the excitonic effects caused by the electron-hole interactions. Nevertheless, by comparing the absorption spectrum of the pristine monolayer to those of doped monolayers, we can achieve a qualitative understanding of the influence of doping on the optical absorption.

**Table 7.** Excitation energies of various peaks appearing in the optical absorption coefficient  $(\alpha(\omega))$  of the pristine GaP monolayer plotted in Fig. 15. MI denotes the most-intense peak.

P			P	0: :				F
Peak	I	II	III	IV	V	VI	VII	VIII
Energy (eV)	2.70	4.16	5.20	5.82(MI)	6.65	7.49	8.32	8.94

The optical absorption coefficients plotted with respect to the energy of the incident photon are presented in Figs. 16 and 17 for Ga(X)P and GaP(Y) systems, respectively. The shaded region of each plot is shown in the inset from which it is clear that in several cases, low-intensity peaks emerge in the lower-energy regions of the spectra. To further illustrate the changes in the absorption spectra due to doping, in Table 8 we present locations of the first  $(E_I)$  and the most-intense peaks  $(E_{MI})$  both for the pristine and the doped monolayers. The changes in  $E_I$  are clearly due to the impurity bands located in the gap region of the pristine monolayer and can be correlated with the modified band gaps of the doped monolayers presented in the Tables 3 and 4. For example,  $E_I = 0.40$  eV for Ga(Zn)P can be understood in terms of its direct band gap of 0.20 eV for the down-spin channel (see Table 3). On the other hand, changes in  $E_{MI}$  are due to global changes in the band structure caused by the dopant atoms.

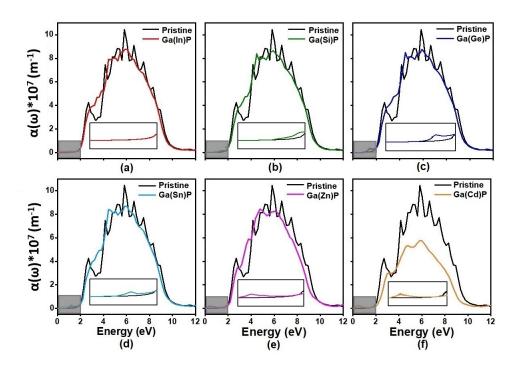


**Figure 16.** Optical absorption coefficient  $(\alpha(\omega))$  as a function of the energy of the incident photon for Ga-substituted monolayers: (a) Ga(In)P, (b) Ga(Si)P, (c) Ga(Ge)P, (d) Ga(Se)P, (e) Ga(Zn)P, and (f) Ga(Cd)P. Shaded regions are shown in inset.

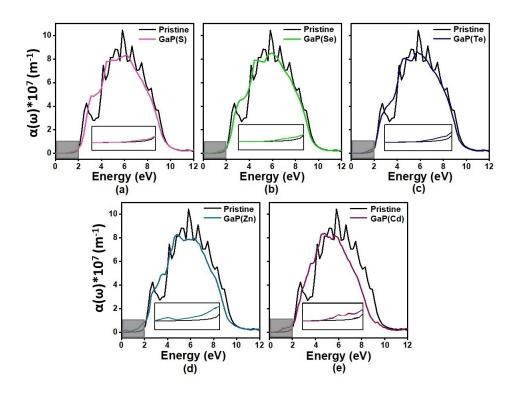


Figure 17. Optical absorption coefficient  $(\alpha(\omega))$  as a function of the energy of the incident photon for P-substituted monolayers: (a) GaP(S), (b) GaP(S), (c) GaP(T), (d) GaP(Z), and (e) GaP(Cd). Shaded regions are shown in inset.

**Table 8.** First peak position  $(E_I)$  and most-intense peak  $(E_{MI})$  in terms of energy for both Ga(X)P and GaP(Y) systems.

$\overline{\mathrm{Ga}(\mathrm{X})\mathrm{P}}$	$E_I(eV)$	$E_{MI}(eV)$	GaP(Y)	$E_I(eV)$	$E_{MI}(eV)$
Pristine	2.70	5.82	Pristine	2.70	5.82
Ga(In)P	3.23	6.03	GaP(S)	4.87	6.22
Ga(Si)P	1.84	5.92	GaP(Se)	1.77	6.00
Ga(Ge)P	1.43	5.9	GaP(Te)	1.83	5.70
Ga(Sn)P	1.21	5.86	GaP(Zn)	0.40	4.80
Ga(Zn)P	0.40	4.77	GaP(Cd)	1.15	4.81
Ga(Cd)P	0.40	5.97			

From Figs. 16 and 17, it is clear that the optical absorption spectra of both the pristine

and doped monolayers cover a wide range of visible and ultraviolet regions making them potential candidates in optoelectronic devices and photovoltaic solar cells. Another interesting aspect of several doped monolayers is the presence of spin-polarized bands with unequal band gaps for the two spin orientations (see Table 3). This suggests the possibility of spin-dependent optical response in these materials which can also be used for device applications.

We have also investigated the above said properties (electronic and optical) by varying the doping percentage from 6.25 % to 2.78 % by using a  $6 \times 6$  supercell, both for the pristine and the doped GaP monolayers. This is done to study the effect of variation of the doping concentration on the said properties. The results of these calculations are discussed in the last section of the SI.

#### 4. Conclusion

To summarize, using a first-principles DFT-based methodology employing the GGA-PBE exchange-correlation functional, we have computationally studied the structural, electronic, magnetic, and optical properties of both pristine and doped GaP monolayers. We find that the pristing monolayer, instead of being completely flat, is periodically buckled with an indirect band gap of 2.15 eV. We considered substitutional doping of the pristine monolayer with a single Ga or P atom of the supercell replaced by the impurity atom, and find that for all doping configurations the resultant monolayers are stable. In several cases the doping led to significant tuning of the band gap, and in one case (In replacing Ga) the band gap transformed into a direct one. Also, doping of some of the impurity elements resulted in induced magnetism due to which the degeneracy of spin up and spin down electrons got lifted, resulting in a spin-polarized band structure. In some of these cases we noted that: (a) band gap of one of the spin orientations was quite small indicating a tendency towards half-metallic behavior, and (b) the band gap corresponding to one of the spins became direct. The former property can be utilized in spintronics while the latter one can be exploited for spin-dependent optics. Thus, we also investigated the optical properties for those doped structures in which for one or both spin orientations the band gap was direct. The obtained optical absorption spectrum spans over wide range of visible and ultraviolet region which suggest its possible applications in solar cells and other optoelectronic devices. Therefore, we believe that doped GaP monolayers can be useful in a wide variety of device applications. Furthermore, given the fact that monolayers have a much larger surface area available as compared to their bulk counterparts, they can also be studied for their catalytic performance. Research along those lines is presently ongoing in our group, and the results will be conveyed in future publications. We also hope that our work will stimulate the experimental activity aimed at synthesizing pristine and doped GaP monolayers.

#### acknowledgments

One of the authors, K.D. acknowledges financial assistance from Prime Minister Research Fellowship (PMRF). R.Y. acknowledges the support through the Institute Post-Doctoral Fellowship (IPDF) of Indian Institute of Technology Bombay.

## References

- [1] Baig N, Kammakakam I and Falath W 2021 *Mater. Adv.* **2**(6) 1821–1871 URL http://dx.doi.org/10.1039/D0MA00807A
- [2] Kolahalam L A, Kasi Viswanath I, Diwakar B S, Govindh B, Reddy V and Murthy Y 2019 Materials Today: Proceedings 18 2182-2190 ISSN 2214-7853 2nd International Conference on Applied Sciences and Technology (ICAST-2019): Material Science URL https://www.sciencedirect.com/science/article/pii/S2214785319325507
- [3] Novoselov K S, Geim A K, Morozov S V, Jiang D e, Zhang Y, Dubonos S V, Grigorieva I V and Firsov A A 2004 Sci. **306** 666–669
- [4] Geim A K and Novoselov K S 2007 Nat. Mater. 6 183–191
- [5] Liu F, Ming P and Li J 2007 Phys. Rev. B **76** 064120–064126
- [6] Shen C and Oyadiji S O 2020 Mater. Today Phys. 15 100257–100283
- [7] Nair R R, Blake P, Grigorenko A N, Novoselov K S, Booth T J, Stauber T, Peres N M and Geim A K 2008 Sci. **320** 1308–1308
- [8] Mas-Balleste R, Gomez-Navarro C, Gomez-Herrero J and Zamora F 2011 Nanoscale 3 20–30
- [9] Zhang X, Hou L, Ciesielski A and Samorì P 2016 Advanced Energy Materials 6 1600671
- [10] Long M, Wang P, Fang H and Hu W 2019 Advanced Functional Materials 29 1803807
- [11] Bhimanapati G R, Lin Z, Meunier V, Jung Y, Cha J, Das S, Xiao D, Son Y, Strano M S, Cooper V R et al. 2015 ACS nano 9 11509–11539
- [12] Schaibley J R, Yu H, Clark G, Rivera P, Ross J S, Seyler K L, Yao W and Xu X 2016 Nature Reviews Materials 1 1–15
- [13] Liu F, Wang C, Sui X, Riaz M A, Xu M, Wei L and Chen Y 2019 Carbon Energy 1 173–199
- [14] Yang Y, Hou H, Zou G, Shi W, Shuai H, Li J and Ji X 2019 Nanoscale 11 16–33
- [15] Yu J, Li J, Zhang W and Chang H 2015 Chemical science 6 6705–6716
- [16] Zhang J, Wang F, Shenoy V B, Tang M and Lou J 2020 Materials Today 40 132–139

- [17] Qiao H, Liu H, Huang Z, Hu R, Ma Q, Zhong J and Qi X 2021 Energy & Environmental Materials 4 522–543
- [18] Akinwande D, Brennan C J, Bunch J S, Egberts P, Felts J R, Gao H, Huang R, Kim J S, Li T, Li Y et al. 2017 Extreme Mechanics Letters 13 42–77
- [19] Thiel L, Wang Z, Tschudin M A, Rohner D, Gutiérrez-Lezama I, Ubrig N, Gibertini M, Giannini E, Morpurgo A F and Maletinsky P 2019 Science 364 973–976
- [20] Yang S, Jiang C and Wei S h 2017 Applied Physics Reviews 4 021304
- [21] Lee W H and Park Y D 2018 Advanced Materials Interfaces 5 1700316
- [22] Mitta S B, Choi M S, Nipane A, Ali F, Kim C, Teherani J T, Hone J and Yoo W J 2020 2D Materials 8 012002
- [23] Restrepo O D, Krymowski K E, Goldberger J and Windl W 2014 New Journal of Physics 16 105009
- [24] Mir S H, Yadav V K and Singh J K 2020 ACS omega 5 14203–14211
- [25] Wu F, Tian H, Shen Y, Zhu Z Q, Liu Y, Hirtz T, Wu R, Gou G, Qiao Y, Yang Y et al. 2022 Advanced Materials Interfaces 9 2200409
- [26] Wild A, Mariani E and Portnoi M E 2022 Physical Review B 105 205306
- [27] Negri M, Francaviglia L, Dumcenco D, Bosi M, Kaplan D, Swaminathan V, Salviati G, Kis A, Fabbri F and Fontcuberta i Morral A 2019 Nano Letters **20** 567–576
- [28] Ye C, Chao D, Shan J, Li H, Davey K and Qiao S Z 2020 Matter 2 323–344
- [29] Sahoo R, Pal A and Pal T 2016 Chemical Communications 52 13528–13542
- [30] Anichini C, Czepa W, Pakulski D, Aliprandi A, Ciesielski A and Samorì P 2018 Chemical Society Reviews 47 4860–4908
- [31] Ahn E C 2020 NPJ 2D Mater. Appl. 4 1–14
- [32] Choudhuri I, Bhauriyal P and Pathak B 2019 Chem. Mater. 31 8260–8285
- [33] Jiang J, Wen Y, Wang H, Yin L, Cheng R, Liu C, Feng L and He J 2021 Advanced Electronic Materials 7 2001125
- [34] Bao X, Ou Q, Xu Z Q, Zhang Y, Bao Q and Zhang H 2018 Advanced Materials Technologies 3 1800072
- [35] Zhang W, Wang Q, Chen Y, Wang Z and Wee A T 2016 2D Materials 3 022001
- [36] Şahin H, Cahangirov S, Topsakal M, Bekaroglu E, Akturk E, Senger R T and Ciraci S 2009 Phys. Rev. B 80 155453–155464

- [37] Zhuang H L, Singh A K and Hennig R G 2013 Phys. Rev. B 87 165415–165422
- [38] Suzuki T 2015 Appl. Phys. Lett. 107 213105–213109
- [39] Lü X, He S, Lian H, Lv S, Shen Y, Dong W and Duan Q 2020 Applied Surface Science 531 147262
- [40] Rouzhahong Y, Wushuer M, Mamat M, Wang Q and Wang Q 2020 Scientific reports 10 1–7
- [41] Liu X F, Luo Z J, Zhou X, Wei J M, Wang Y, Guo X, Lv B and Ding Z 2019 Chinese Physics B 28 086105
- [42] Nowak C, Chassé A, Hempelmann A, Richter W, Dudzik E, Whittle R, McGovern I, Braun W and Zahn D 1994 Surface science 307 685–690
- [43] Zhao J, Zeng H and Yao G 2021 Physical Chemistry Chemical Physics 23 3771–3778
- [44] Wang Y and Shi S 2010 Solid State Communications 150 1473–1478
- [45] Singla P, Goel N, Singhal S et al. 2015 Ceram. Int. 41 10565–10577
- [46] Tsipas P, Kassavetis S, Tsoutsou D, Xenogiannopoulou E, Golias E, Giamini S, Grazianetti C, Chiappe D, Molle A, Fanciulli M et al. 2013 Appl. Phys. Lett. 103 251605–251609
- [47] Koratkar N A 2016 Nat. Mater. 15 1153–1154
- [48] Dai J, Yang T, Jin Z, Zhong Y, Hu X, Zou J, Xu W, Li T, Lin Y, Zhang X et al. 2022 Nano Res. 15 9954–9959
- [49] Li D and Yu J 2021 Physica E: Low-dimensional Systems and Nanostructures 126 114480
- [50] Al Balushi Z Y, Wang K, Ghosh R K, Vilá R A, Eichfeld S M, Caldwell J D, Qin X, Lin Y C, DeSario P A, Stone G et al. 2016 Nature materials 15 1166–1171
- [51] Chen C, Meng F and Song J 2016 Journal of Applied Physics 119 064302
- [52] Xia C, Peng Y, Wei S and Jia Y 2013 Acta materialia 61 7720–7725
- [53] Chen G X, Li H F, Wang D D, Li S Q, Fan X B and Zhang J M 2019 Vacuum 165 35–45
- [54] Cui Z, Bai K, Wang X, Li E and Zheng J 2020 Physica E: Low-dimensional Systems and Nanostructures 118 113871
- [55] Du K, Xiong Z, Ao L and Chen L 2021 Vacuum 185 110008
- [56] Baur B, Steinhoff G, Hernando J, Purrucker O, Tanaka M, Nickel B, Stutzmann M and Eickhoff M 2005 Applied Physics Letters 87 263901
- [57] Xu D, He H, Pandey R and Karna S P 2013 Journal of Physics: Condensed Matter 25 345302
- [58] Shu H, Niu X, Ding X and Wang Y 2019 Applied Surface Science 479 475–481

- [59] Bahuguna B P, Saini L, Sharma R O and Tiwari B 2018 Physica E: Low-dimensional Systems and Nanostructures 99 236–243
- [60] Peng Q, Chen X J, Liu S and De S 2013 RSC Adv. 3(19) 7083-7092 URL http://dx.doi. org/10.1039/C3RA40841H
- [61] Beshkova M and Yakimova R 2020 Vacuum 176 109231
- [62] Aparna A, Brahmajirao V and Karthikeyan T 2014 Procedia materials science 6 1650–1657
- [63] Treece R E, Macala G S and Kaner R B 1992 Chemistry of materials 4 9–11
- [64] Václavík J and Vápenka D 2013 Gallium phosphide as a material for visible and infrared optics *EPJ Web of Conferences* vol 48 (EDP Sciences) p 00028
- [65] Wight D 1977 Journal of Physics D: Applied Physics 10 431
- [66] Zipperian T and Dawson L 1981 Applied Physics Letters 39 895–897
- [67] Lu X, Huang S, Diaz M B, Kotulak N, Hao R, Opila R and Barnett A 2012 IEEE Journal of Photovoltaics 2 214–220
- [68] Singh S and Srivastava P 2013 Applied Nanoscience 3 89–94
- [69] Emmer H, Chen C T, Saive R, Friedrich D, Horie Y, Arbabi A, Faraon A and Atwater H A 2017 Scientific reports 7 1–6
- [70] Mori H, Ogasawara M, Yamamoto M and Tachikawa M 1987 Applied physics letters 51 1245–1247
- [71] Tilmann B, Grinblat G, Berté R, Özcan M, Kunzelmann V F, Nickel B, Sharp I D, Cortés E, Maier S A and Li Y 2020 Nanoscale Horizons 5 1500–1508
- [72] Ren M, Li M, Zhang C, Yuan M, Li P, Li F, Ji W and Chen X 2016 Solid State Communications 239 32–36
- [73] Kumar V, Shah E V and Roy D R 2016 Electronic properties of hexagonal gallium phosphide: A DFT investigation AIP Conf. Proc. vol 1731 (AIP Publishing LLC) pp 120026–120029
- [74] Akbari A, Naseri M and Jalilian J 2018 Chem. Phys. Lett. **691** 181–189
- [75] Ma X, Fan Z, Wu J, Jiang X and Chen J 2018 Computational design of silicon contacts on 2D transition-metal dichalcogenides: the roles of crystalline orientation, doping level, passivation and interfacial layer 2018 IEEE International Electron Devices Meeting (IEDM) (IEEE) pp 24–27
- [76] Liu C, Wang Q, Jia F and Song S 2019 J. Mol. Liq. 292 111390–111400
- [77] Zhang Y, Mascarenhas A, Xin H and Tu C 2000 Phys. Rev. B 61 7479–7482

- [78] Hahn J and Kang H 1999 Phys. Rev. B 60 6007–6017
- [79] Hart J L, Hantanasirisakul K, Lang A C, Anasori B, Pinto D, Pivak Y, van Omme J T, May S J, Gogotsi Y and Taheri M L 2019 *Nat. Commun.* **10** 1–10
- [80] Liu Z, Lau S P and Yan F 2015 Chem. Soc. Rev. 44 5638–5679
- [81] Hohenberg P and Kohn W 1964 Phys. Rev. 136–143 B864
- [82] Kohn W and Sham L J 1965 Phys. Rev. 140 A1133–A1138
- [83] Kresse G and Furthmüller J 1996 Comput. Mater. Sci. 6 15–50
- [84] Kresse G and Furthmüller J 1996 Phys. Rev. B 54 11169–11204
- [85] Perdew J P, Burke K and Ernzerhof M 1996 Phys. Rev. Lett. 77 3865–3868
- [86] Kresse G and Joubert D 1999 Phys. Rev. B 59 1758–1775
- [87] Blöchl P E 1994 Phys. Rev. B **50** 17953–17979
- [88] Monkhorst H J and Pack J D 1976 Phys. Rev. B 13 5188–5192
- [89] Heyd J, Scuseria G E and Ernzerhof M 2003 The Journal of chemical physics 118 8207–8215
- [90] Kresse G and Hafner J 1994 Phys. Rev. B 49(20) 14251-14269 URL https://link.aps. org/doi/10.1103/PhysRevB.49.14251
- [91] Grimme S, Antony J, Ehrlich S and Krieg H 2010 J. Chem. Phys. 132 154104–154123
- [92] Tang W, Sanville E and Henkelman G 2009 J. Phys. Condens. Matter 21 084204
- [93] Chabi S, Guler Z, Brearley A J, Benavidez A D and Luk T S 2021 Nanomaterials 11 ISSN 2079-4991 URL https://www.mdpi.com/2079-4991/11/7/1799
- [94] Ullah S, Denis P A, Menezes M G, Sato F and Capaz R B 2020 *Phys. Rev. B* **102**(13) 134112 URL https://link.aps.org/doi/10.1103/PhysRevB.102.134112
- [95] Asghar M, Ullah H, Iqbal M W and Shin Y H 2022 Materials Science in Semiconductor Processing 152 107049 ISSN 1369-8001 URL https://www.sciencedirect.com/science/ article/pii/S1369800122005789
- [96] Asghar M, Ullah H, Iqbal M W, Shin Y H and Neffati R 2023 Materials Today Communications 35 106124 ISSN 2352-4928 URL https://www.sciencedirect.com/ science/article/pii/S2352492823008152
- [97] Waheed H S, Ullah H, Shin Y H and Alanazi Y M 2023 physica status solidi (b) 260 2300028– 2300036
- [98] Waheed H S, Asghar M, Ahmad H S, Abbas T, Ullah H, Ali R, Khan M J I, Iqbal M W, Shin Y H, Khan M S et al. 2023 physica status solidi (b) 260 2200267

- [99] Gul S H, Ali B, Shafiq M, Idrees M and Amin B 2023 Journal of Solid State Chemistry 326 124187 ISSN 0022-4596 URL https://www.sciencedirect.com/science/article/pii/S0022459623003559
- [100] Nosé S 1984 The Journal of chemical physics 81 511–519
- [101] Sethulakshmi N, Mishra A, Ajayan P M, Kawazoe Y, Roy A K, Singh A K and Tiwary C S 2019 Mater. Today. 27 107–122
- [102] Zheng H, Zhang J, Yang B, Du X and Yan Y 2015 Phys. Chem. Chem. Phys. 17 16341–16350
- [103] Lu W and Lieber C M 2007 Nat. Mater. 6 841–850
- [104] Cutkosky R E 1954 *Phys. Rev.* **96**(4) 1135-1141 URL https://link.aps.org/doi/10. 1103/PhysRev.96.1135
- [105] Idrees M, Khurami M, Amin B, Chen Y and Yan X 2023 Materials Science in Semiconductor Processing 163 107593 ISSN 1369-8001 URL https://www.sciencedirect.com/science/ article/pii/S136980012300286X
- [106] Khurami M, Amin B, Chen Y, Yan X and Idrees M 2023 Solid State Communications 371 115273 ISSN 0038-1098 URL https://www.sciencedirect.com/science/article/pii/S0038109823002107
- [107] Deb J, Paul D and Sarkar U 2020 J. Mater. Chem. C . 8 16143–16150
- [108] Jain M, Singh A, Basera P, Kumar M and Bhattacharya S 2020 J. Mater. Chem. C . 8 10362-10368